UCME_A_1082678 TFJATS_StdSerif-800.cls June 1, 2016 16:39 Trim Info: 8.5in × 11in

UCME #1082678, VOL 0, ISS 0

Viscoelectromechanics modeling of intestine wall hyperelasticity

Alessio Gizzi, Anna Pandolfi, and Marcello Vasta

QUERY SHEET

This page lists questions we have about your paper. The numbers displayed at left can be found in the text of the paper for reference. In addition, please review your paper as a whole for correctness.

There are no Editor Queries for this paper.

TABLE OF CONTENTS LISTING

The table of contents for the journal will list your paper exactly as it appears below:

UCME_A_1082678 TFJATS_StdSerif-800.cls June 1, 2016 16:39 Trim Info: 8.5in × 11in

INTERNATIONAL JOURNAL FOR COMPUTATIONAL METHODS IN ENGINEERING SCIENCE AND MECHANICS
2016, VOL. 0, NO. 0, 1–13
http://dx.doi.org/10.1080/15502287.2015.1082678

Viscoelectromechanics modeling of intestine wall hyperelasticity

Alessio Gizzi[a], Anna Pandolfi[b], and Marcello Vasta[c]

[a]Engineering Department, University Campus Bio-Medico of Rome, via A. del Portillo 21, Rome, Italy; [b]Politecnico di Milano, Dipartimento di Ingegneria Civile ed Ambientale, Piazza Leonardo da Vinci 32, Milano, Italy; [c]Dipartimento INGEO, Università di Chieti-Pescara, Viale Pindaro 42, Pescara, Italy

ABSTRACT

Elastic-electroactive biological media are sensitive to both mechanical and electric forces. Their active behavior is often associated with the presence of reinforcing fibers and their excitation-contraction coupling is due to the interplay between the passive elastic tissue and the active muscular network. In this paper we focus on the theoretical framework of constitutive equations for viscous electroactive media. The approach is based on the additive decomposition of the Helmholtz free energy accompanied to the multiplicative decomposition of the deformation gradient in elastic, viscous and active parts. We describe a thermodynamically sound scenario that accounts for geometric and material nonlinearities.

KEYWORDS

Active electromechanics; Biomechanics; Multiplicative decomposition of the deformation gradient; Viscohyperelasticity

1. Introduction

The term elastic-electroactive (EA) media refers to a wide range of materials and physical systems which are sensitive to mechanical forces and electric fields. Piezoelectric crystals [1] and electroactive polymers [2–5] are the two most studied macroclasses of EA systems, but recently the active electromechanical coupling has been extended to the less explored world of biological tissues [6]. A common feature of EA media is the ability to spontaneously deform upon the application of an electric field and to show a mechanoelectric feedback (MEF) when mechanical forces are applied. The latter behavior is likely due to the modification of the original configuration of the electric field caused by the deformation of the system and in some cases to induced anisotropy of the material [7–9].

Soft active materials often exhibit rate dependent behaviors at different scales [10, 11]: stress relaxation at constant strain, creep at constant stress, hysteresis during loading and unloading, strain-rate dependence. For most biological materials, the viscoelastic response is due to the interactions between proteoglycans in the ground substance and the reinforcing collagen fibers. For example, cartilage—mainly made of water ($\sim$ 75%), collagen fibers, and extracellular matrix—and trabecular bone show viscoelastic properties due to fluid flow during loading; intervertebral discs ($\sim$ 78% of water) show viscoelasticity due to fluid flow during loading and shear forces between matrix and fibers during fiber straightening. Viscous behaviors are motivated biologically by the protection against the injuries that can be induced by fast actions and are justified physiologically by the composite structure of the tissues [12].

When the involved deformations are small and the materials are linear elastic, viscosity can be described with linear theories, using mechanical rheological analogs or Boltzmann' superposition principle. Idealized mechanical analogs, based on simplified reological components, can be used to describe also nonlinear viscoelastic materials: the generalized Maxwell model, which is an extension of the standard solid model, is often adopted to describe viscosity within finite kinematics. A promising approach that allows to incorporate viscoelastic behaviors in a sound thermodynamical framework relies on the introduction of dissipation potentials [13]. Starting from a generalized theory of viscoelasticity [14], recent contributions on the topic have been developed in the context of soft electroactive polymers [3–5, 15, 16]. Furthermore, viscosity in multiphysics coupling and viscomagnetomechanical effects have also been proposed [17–19].

In spite of the vast literature on the subject [20–22], the role of viscous stresses on electric fields and the reverse feedback lack of accurate consideration, in particular when their mutual interactions need to be accounted for, as in the case of anisotropic active biological media. In view of tackling this particular aspect, in this work we discuss a general theoretical framework for active viscoelasticity in fiber reinforced tissues, and apply the theory to the numerical simulation of the peristalsis in a portion of the human intestine.

CONTACT Alessio Gizzi a.gizzi@unicampus.it University Campus Bio-Medico of Rome, Engineering Department, via A. del Portillo 21, 00128 Rome, Italy.
Color versions of one or more of the figures in the article can be found online at www.tandfonline.com/ucme.

On the wake of two decades of intense experimental and modeling research, in this work we aim at clarifying the thermodynamical basis of multiphysics modeling in soft excitable tissues. Experimental evidence has shown important differences in the pattern of peristaltic wave propagation along the intestine. In particular, variations in the pacemaker site and correspondingly in speed, direction, and extension of excitation have been recorded in vivo. Slow waves, and longitudinal and circular action potentials, showing their characteristic propagation pattern, have been detected [23]. The observation of abnormal propagating waves in smooth muscle organs other than the heart allowed to generalize and extend the concept of arrhythmias and reentrant excitations [24].

The paper is organized as follows. Section 2 describes briefly the biophysics of the human wall intestine, while Section 3 presents a general theoretical framework of the viscoelectroactive mechanical problem. In Section 4 the constitutive relationships are described by decoupling the Helmholtz free energy according to a multiplicative decomposition of the deformation gradient. By the way of a case study and using a simplified model of the intestine electrophysiology, in Section 5 we present an illustrative simulation of peristaltic contraction, in a portion of human colon reconstructed from virtual colonoscopy images. In Section 6 limitations and future perspective are discussed.

2. Biophysics of intestine

Human intestine belongs to the class of excitable deformable tissues responding differently upon isotonic, isometric or dynamic conditions. Gastrointestine (GI) wall, in particular, is a very complex system consisting of four main layers with definite and peculiar structures: (i) mucosa, (ii) submucosa, (iii) circular muscularis (CM) and longitudinal muscularis (LM), and (iv) serosa. For the purpose of the present work, in the following we consider the sole muscularis layer. Intestine peristaltic activity in the muscularis layer is a complex phenomenon that involves excitable and deformable cells, called smooth muscle cells (SMC). Muscle contraction, in particular, is characterized by multiple superposed time-dependent phenomena at the microscale which render the chemo-mechanical reaction process markedly dependent on the typical frequency of the system [25].

GI wall anatomy and function. The contractile properties of SMCs are the result of the interaction of actin and myosin filaments; see Figure 1. SMC contraction is activated by the migration of calcium ions supplied by hydrolysis processes. SMC protein filaments show a specific spatial organization within the intestine wall which allows for contraction up to 80% of their resting length. Moreover, SMCs contract at a very low frequency and exert force for long times. This aspect is

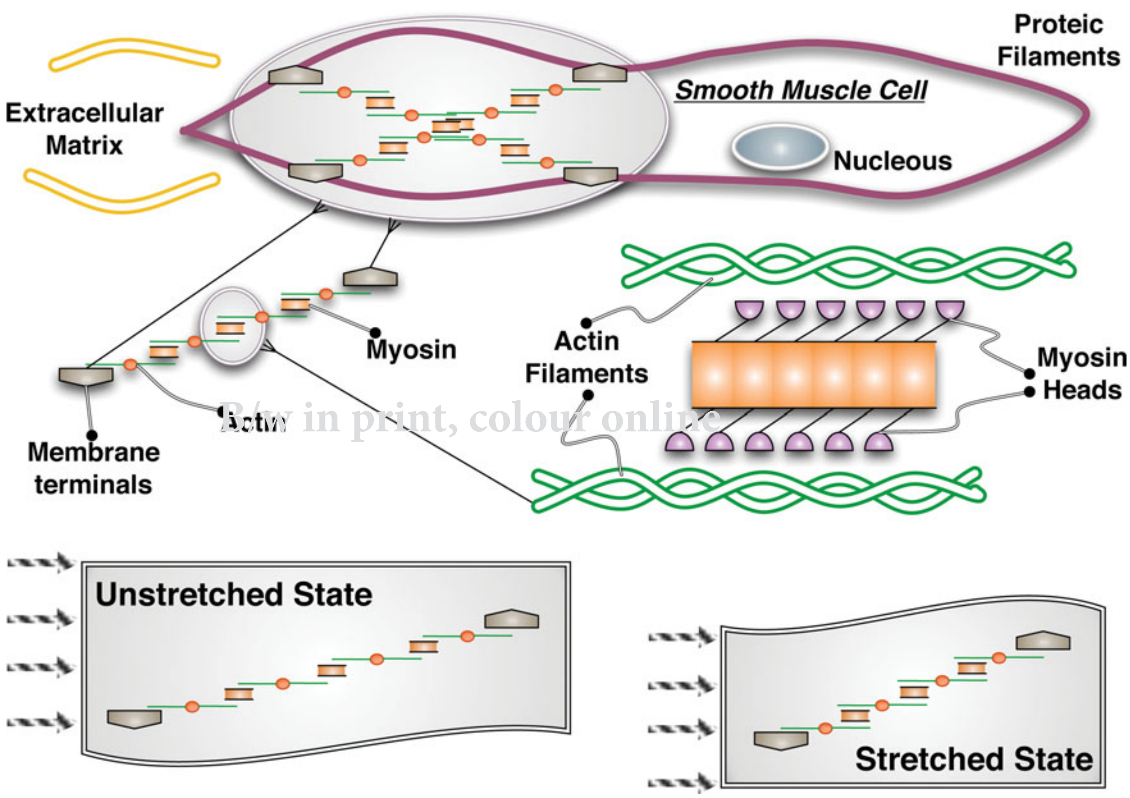

Figure 1. Schematic representation of the smooth muscle cells. Internal contractile structures cartoon description in the material and activated states.

energetically fundamental for reducing the overall continuous dissipation.

SMC within the intestine wall are grouped in bundles of about 1,000 fibers and arranged in two preferential orientations, e.g., longitudinal (ML) or circumferential (MC). Fibers are highly interconnected in the bundle and with other bundles, in order to spread the bioelectrical potentials efficiently. The resulting structure is a functional syncytium, typical of electroactive biological tissues, able to support reaction-diffusion processes with associated propagating behaviors [26, 27]. Additionally, ML and MC bundles show connection points that enable correct peristaltic sequences.

Electrophysiology. The electrical activity of intestine is characterized by slow waves and superimposed fast spikes. Slow waves, characterized by a frequency of 3–12 oscillations per minute, wavelength of 5–10 cm, an average duration of 6 s, and voltage membrane oscillations of 5–15 mV, are fundamental to regulate GI contractility. The interstitial cells of Cajal (ICC) form a specialized SMC pacing system responsible of the slow wave generation and propagation together with the nervous system [28]. ICC are located between the longitudinal and circumferential muscularis and are organized in a homogeneous network. Interestingly, slow wave oscillations are present along the whole intestine also when contractions are not present, but their frequency gradually reduces in the aboral direction. Fast spiking waves are real voltage action potentials (AP) signals that appear during the contraction of the intestine walls. Fast spike onset superposes to slow waves when a threshold of about −40 mV is reached, and are characterized by a frequency of 1–10 Hz and a duration of 10–20 ms.

Consequently to the presence of the two electric signals, the electromechanical behavior of the GI system is very sensitive to small variations of the resting membrane potential, and several chemical, electrical and mechanical factors can modify this state, e.g., acetylcholine, noradrenaline and sympathetic stimulations, intestine wall stretching (stretch activated channels), and temperature changes [29].

Movements & contractions. The contraction of the GI apparatus is driven by the electric peristaltic motion. Peristaltic waves propagate in an anterograde direction with a velocity of 0.5–2 cm/min, showing deceleration from the proximal to the distal intestine. In the small intestine, for example, the mean wave velocity is 1 cm/min and requires 3–5 hours to move the chime from the pylorus to the ileocaecal valve. Peristaltic movements are fundamental to obtain a calibrated mix of the chime, since different actions have to take place in different portions of the GI system with specific timings. The overall phenomenon of chime motion is known as migrant motor complex (MMC).

3. Active electromechanical model formulation

We refer to a body of reference mass density per unit volume ρ_0 undergoing a motion $\boldsymbol{x} = \boldsymbol{x}(\boldsymbol{X}, t)$, where $\boldsymbol{X}$ are the coordinates in the material configuration and $\boldsymbol{x}$ are the coordinates in the spatial configuration. The volume and the boundary with outward normal $\boldsymbol{N}$ in the material configuration are denoted by Ω_0 and $\partial\Omega_0$, respectively. We denote with $\boldsymbol{F} = \nabla_X \boldsymbol{x}$ the deformation gradient, with $\boldsymbol{C} = \boldsymbol{F}^T\boldsymbol{F}$ the Cauchy-Green deformation tensor, and with ρ the mass density per unit current volume. The local form of the mass balance and of the linear momentum read

$$\det \boldsymbol{F} = J = \frac{\rho_0}{\rho}, \qquad \rho_0 \frac{d\boldsymbol{V}}{dt} = \nabla_X \cdot \boldsymbol{P} + \rho_0 \boldsymbol{B}, \tag{1}$$

where $\boldsymbol{B}$ are the body forces per unit of mass, $\boldsymbol{V}$ is the material velocity, $\boldsymbol{P}$ the first Piola-Kirchhoff stress tensor, and $\nabla_X \cdot$ the material divergence operator. The angular momentum balance is satisfied through the symmetry of the product $\boldsymbol{P}\boldsymbol{F}^T = \boldsymbol{F}\boldsymbol{P}^T$ and the boundary tractions $\boldsymbol{T}$ are expressed through the Cauchy's relation $\boldsymbol{T} = \boldsymbol{P}\boldsymbol{N}$.

Denoting $\boldsymbol{E}$, $\boldsymbol{D}$, and $\boldsymbol{\Pi}$ the material electric field, the material electric induction, and the material polarization density, respectively, and assuming, as usual, that the material electric field is the gradient of the electric potential φ

$$\boldsymbol{E} = -\frac{\partial \varphi}{\partial \boldsymbol{X}} = -\nabla_X \varphi,$$

the equations of electrostatics in material form read

$$\nabla_X \times \boldsymbol{E} = \boldsymbol{0}, \qquad \nabla_X \cdot \boldsymbol{D} = 0,$$

where $\nabla_X \times$ denotes the material curl operator. The material electric induction, in particular, is given as

$$\boldsymbol{D} = J\epsilon_0 \boldsymbol{C}^{-1}\boldsymbol{E} + \boldsymbol{\Pi}, \tag{2}$$

where ϵ_0 is the dielectric constant of the vacuum. The first term in (2) accounts for electric field distortions due to material deformations while the polarization tensor $\boldsymbol{\Pi}$ must be characterized via a constitutive relationship.

Electrophysiology is governed by the electric current balance, a reaction-diffusion equation known as cable equation. The local material form is given by

$$C_E \frac{\mathrm{D}\varphi}{\mathrm{D}t} = -\frac{1}{J}\nabla_X \cdot \boldsymbol{H}_E + I_E, \tag{3}$$

where C_E is the electric capacitance, I_E the total ionic transmembrane current, and $\boldsymbol{H}_E$ the electric flux. The material time derivative of the electric potential is defined as

$$\frac{D\varphi}{Dt} = \frac{\partial \varphi}{\partial t} + \frac{d\boldsymbol{X}}{dt} \cdot \nabla_{\boldsymbol{X}} \varphi.$$

According to a standard notation, the symbol $\cdot$ denotes the scalar product. Boundary conditions are expressed as $-[[\boldsymbol{H}_E]] \cdot \boldsymbol{N} = \omega$, where ω denotes the surface charge density in the material configuration, while the electric flux is assumed to follow a linear dependence on the gradient of the electric potential (Fick's law)

$$\boldsymbol{H}_E = -J\boldsymbol{K}_E \nabla_{\boldsymbol{X}} \varphi,$$

where $\boldsymbol{K}_E$ denotes a material second-order tensor of electric conductivities.

In order to setup a thermodynamic approach to the electromechanical problem, we begin by introducing a specific internal energy U of the system dependent also on the electric field [30]. Accounting for the mass and the linear momentum balances (1), and using the superposed dot to denote the rate of a quantity, the local form of the rate energy balance becomes

$$\dot{U} = \boldsymbol{P} : \dot{\boldsymbol{F}} + \boldsymbol{E} \cdot \dot{\boldsymbol{D}} + \rho_0 Q - \nabla_{\boldsymbol{X}} \cdot \boldsymbol{H}_T, \tag{4}$$

where $\dot{U}$ is the specific rate of the internal energy, Q the heat supply per unit mass, and $\boldsymbol{H}_T$ the material energy flux vector. In turn, the dissipation inequality assumes the form [1]

$$T\dot{\Gamma} = T\dot{N} - U + \boldsymbol{E} \cdot \dot{\boldsymbol{D}} + \boldsymbol{P} : \dot{\boldsymbol{F}} - \frac{1}{T}\boldsymbol{H}_T \cdot \nabla_{\boldsymbol{X}} T \geq 0, \tag{5}$$

where $\dot{\Gamma}$ denotes the total entropy production, $\dot{N}$ the rate of entropy production per unit reference volume, T is the temperature, and $:$ denotes the contraction between tensors.

4. Constitutive relations for active media

We follow a sound thermodynamical approach [31–33] and assume that the local thermodynamic state of the body B_0 is completely defined by the deformation gradient $\boldsymbol{F}$, temperature T, electric field $\boldsymbol{E}$, and by a set of internal variables $\boldsymbol{Q}$. In the present context, internal variables are included to consider the presence of viscosity and will be specified according to the material model and to the dissipative process considered.

We depart from the alternative Helmholtz thermodynamic potential A, a Legendre transform of the internal energy potential, which, in turn, is a function of the state variables

$$A = U - \boldsymbol{D} \cdot \boldsymbol{E} - TN = A(\boldsymbol{F}, T, \boldsymbol{E}, \boldsymbol{Q}) \tag{6}$$

and consider the total stress $\boldsymbol{P}$ as the sum of an equilibrium stress $\boldsymbol{P}^E$, function of the state variables, and a viscous stress $\boldsymbol{P}^v$, which additionally depends on the rate of deformation $\dot{\boldsymbol{F}}$, i.e.,

$$\boldsymbol{P}(\boldsymbol{F}, T, \boldsymbol{E}, \boldsymbol{Q}; \dot{\boldsymbol{F}}) \equiv \boldsymbol{P}^E(\boldsymbol{F}, T, \boldsymbol{E}, \boldsymbol{Q}) + \boldsymbol{P}^v(\boldsymbol{F}, T, \boldsymbol{E}, \boldsymbol{Q}; \dot{\boldsymbol{F}}). \tag{7}$$

$\boldsymbol{P}^E$ is defined as the total stress when no deformation rate is present:

$$\boldsymbol{P}^E(\boldsymbol{F}, T, \boldsymbol{E}, \boldsymbol{Q}) \equiv \boldsymbol{P}(\boldsymbol{F}, T, \boldsymbol{E}, \boldsymbol{Q}; \boldsymbol{0}).$$

Following the standard variational procedure, the constitutive equations derive as

$$\boldsymbol{P}^E = \partial_{\boldsymbol{F}} A(\boldsymbol{F}, T, \boldsymbol{E}, \boldsymbol{Q}), \quad N = \partial_T A(\boldsymbol{F}, T, \boldsymbol{E}, \boldsymbol{Q}),$$
$$\boldsymbol{D} = -\partial_{\boldsymbol{E}} A(\boldsymbol{F}, T, \boldsymbol{E}, \boldsymbol{Q}),$$

with the thermodynamic forces $\boldsymbol{Y}$ conjugate to the internal variables defined as

$$\boldsymbol{Y} \equiv -\partial_{\boldsymbol{Q}} A(\boldsymbol{F}, T, \boldsymbol{E}, \boldsymbol{Q}).$$

The thermodynamic framework is then completed with the introduction of kinetic relations for $\boldsymbol{P}^v$ and $\dot{\boldsymbol{Q}}$ [34, 35]. We conveniently introduce a dual dissipation potential ψ^* dependent on the deformation rates $\dot{\boldsymbol{F}}$, such that the viscous stress derives as

$$\boldsymbol{P}^v = \partial_{\dot{\boldsymbol{F}}} \psi^*(\boldsymbol{F}, T, \boldsymbol{E}, \boldsymbol{Q}; \dot{\boldsymbol{F}}). \tag{8}$$

The functional form of the dual dissipation potential is chosen according to the kind of viscosity considered, as long as it is convex in order to satisfy the sign of the dissipation inequality [35].

Since in the following we refer to isothermal processes, in all the successive equations we drop the dependence on the temperature T.

4.1. A general Helmholtz potential for active electromechanics

As customary for a system undergoing multiphysics processes in finite deformations, we adopt the multiplicative decomposition of the deformation gradient as the most convenient mathematical representation of the change of the system's configuration [9, 36–38]. In view of modeling the viscous-active coupling, we start from the assumption that the deformation gradient decomposes into elastic $\boldsymbol{F}^e$ and active $\boldsymbol{F}^a$ parts [6]; see Figure 2a. But instead of considering a purely elastic behavior of the material, we introduce viscosity, described schematically by the standard solid equivalent model shown in Figure 2b. Thus,

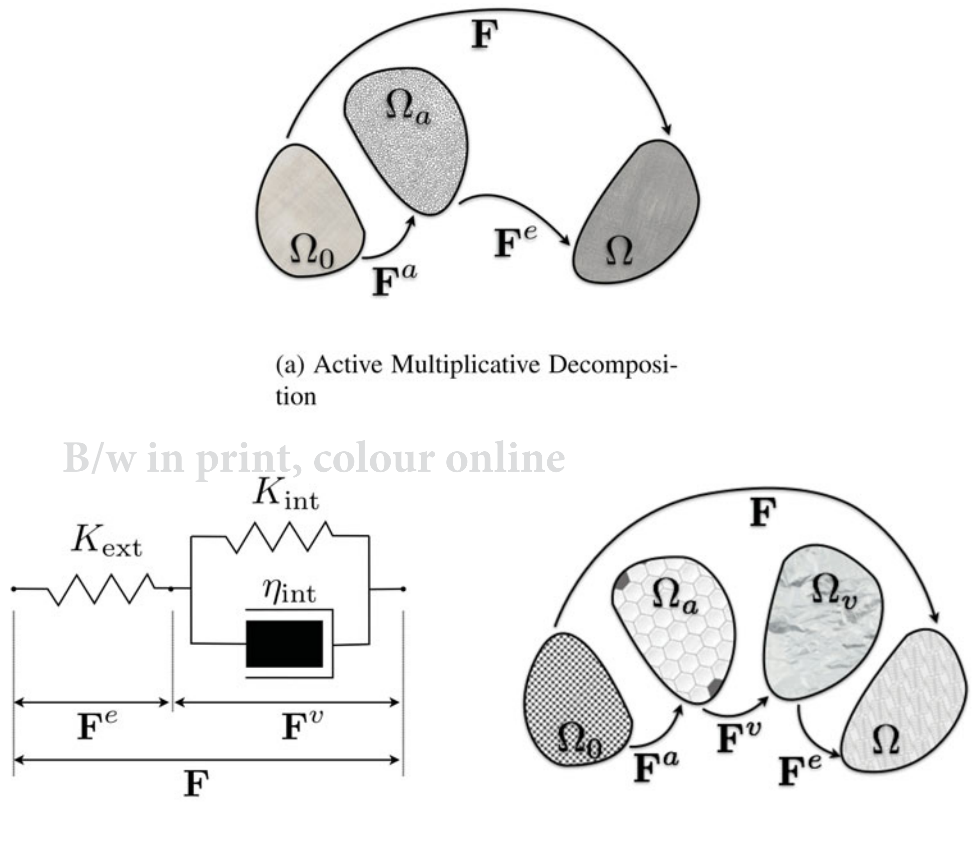

(a) Active Multiplicative Decomposition

B/w in print, colour online

(b) Viscous Model

(c) Full Multiplicative Decomposition

Figure 2. (a) Sketch of the multiplicative decomposition of the deformation gradient tensor in elastic and active part for an inviscid hyper-elastic model. (b) Schematic representation of the reological equivalent standard solid model for the viscous behavior. (c) Sketch of the multiplicative decomposition of the deformation gradient tensor in elastic, viscous and active part.

we replace the elastic deformation gradient with the product between an elastic deformation gradient $\boldsymbol{F}^e$ and a viscous deformation gradient $\boldsymbol{F}^v$, that will account for rate-dependency; see Figure 2c:

$$\boldsymbol{F} = \boldsymbol{F}^e \boldsymbol{F}^v \boldsymbol{F}^a. \tag{9}$$

The elastic part of the deformation gradient is related to the passive response of the material, while the active part is introduced to describe the geometrical changes induced by the electric field on unconstrained portions of the material. The viscous deformation gradient, which is naturally dependent on time, can be considered as an internal variable $\boldsymbol{F}^v \equiv \mathbf{Q}$, and its evolution will be governed by suitable kinetic relations. Assumption (9) introduces multiple ideal intermediate non compatible configurations where a single inelastic phenomenon takes place without inducing stresses in the continuum [35]. The compatibility requirement will relax the body from the last intermediate configuration to the current configuration, where equilibrium and compatibility conditions are fully satisfied.

In the view of reducing the complexity of the nonlinearities of the constitutive description, the Helmholtz free energy can be conveniently split into the sum of three distinct contributions (elastic, viscous, and active) by assuming a full separation of the arguments. This choice, motivated by the physical distinction between passive, viscous, and active behaviors, allows to maintain in each contribution the functional dependency on the state variables obtained in the absence of other behaviors. In particular, when the approach is adopted in the hyperelastic modeling of multiscale and multiphysics media, only the elastic contribution to the free energy density is considered a function of the elastic deformation gradient [35, 39]. Thus, we assume the additive decomposition of the free energy density in three contributions in the form

$$A(\boldsymbol{F}^e, \boldsymbol{F}, \boldsymbol{E}, \boldsymbol{F}^v) = A^e(\boldsymbol{F}^e) + A^v(\boldsymbol{F}^v) + A^a(\boldsymbol{F}, \boldsymbol{E}). \tag{10}$$

The term A^e represents the classical strain energy density of hyperelastic materials, while A^v is a dissipative term that describes viscous phenomena and must be related to a time interval. The term A^a, instead, is an inelastic free energy density that accounts for the electric field and for all its effects, including inelastic deformations. From assumptions (9)–(10), the equilibrium stress $\boldsymbol{P}^E$ and the thermodynamic forces $\boldsymbol{Y}$ follow as

$$\boldsymbol{P}^E = \boldsymbol{P}^p + \boldsymbol{P}^a, \qquad \boldsymbol{Y} = -\partial_{\boldsymbol{F}^v} A = -\boldsymbol{Y}^e - \boldsymbol{Y}^v - \boldsymbol{Y}^a . \tag{11}$$

The thermodynamic framework allows us to clearly distinguish between a passive stress $\boldsymbol{P}^p$

$$\boldsymbol{P}^p = \partial_{\boldsymbol{F}^e} A^e(\boldsymbol{F}^e)\, \partial_{\boldsymbol{F}} \boldsymbol{F}^e = \boldsymbol{P}^e \boldsymbol{F}^{v-T} \boldsymbol{F}^{a-T},$$

and an active stress $\boldsymbol{P}^a$

$$\boldsymbol{P}^a = \partial_{\boldsymbol{F}} A^a(\boldsymbol{F}, \boldsymbol{E}),$$

where we denote with ^{T} ($^{-T}$) the transpose (inverse of the transpose). The stress $\boldsymbol{P}^p$ derives from the strain energy density A^e, which in the intermediate configuration defines the elastic stress $\boldsymbol{P}^e$, work-conjugate to $\boldsymbol{F}^e$. The active stress $\boldsymbol{P}^a$ is originated by the inelastic part A^a of the free energy. The choice of the expression A^a is intrinsically linked to the definition of the $\boldsymbol{F}^a$. In turn, $\boldsymbol{F}^a$ must be chosen according to the micro- and macrocharacteristics of the material, including the underlying microstructure. As previously mentioned, the kinetic equations for the evolution of the viscous stress are derived from a dual dissipation potential ψ^*, which can be dependent on the viscous rate of deformation $\boldsymbol{D}^v$ and possibly on the electric field $\boldsymbol{E}$:

$$\boldsymbol{P}^v = \partial_{\dot{\boldsymbol{F}}^v} \psi^*(\boldsymbol{D}^v, \boldsymbol{E}) . \tag{12}$$

The deformation rate $\boldsymbol{D}^v$ is defined as

$$\boldsymbol{D}^v = \frac{1}{2}\left(\dot{\boldsymbol{F}}^v \boldsymbol{F}^{v-1} + \boldsymbol{F}^{v-T} \dot{\boldsymbol{F}}^{v\,T}\right) .$$

Once the dissipation potential has been assigned, the viscous potential can be evaluated within a time interval Δt as (see Appendix A for details)

$$A^v(\boldsymbol{F}^v, \boldsymbol{E}) \approx \Delta t\, \psi^*(\boldsymbol{D}^v, \boldsymbol{E}) .$$

Upon finite element discretization, the active viscoelastic problem requires the solution of the nonlinear semidiscrete balance equation $(1)_2$ and reaction-diffusion equation (3) at assigned time steps t_i. In the present approach, we make recourse to a staggered method and solve separately the reaction-diffusion equation, by assuming a rigid solid, and the linear momentum equation. Time integration of the reaction-diffusion equation is achieved by means of an explicit parabolic algorithm, with time steps sufficiently small to satisfy the Levy-Courant stability conditions. For the chosen mesh size, with $h_{\min} = 0.035$ mm, the time step was $\Delta t = 0.0059$ ms. The resulting electric field is used to solve explicitly the balance equation through a dynamic-relaxation algorithm [40, 41]. Within each iteration of the dynamic-relaxation algorithm, the state variables attendant the constitutive behavior are evaluated using a variational approach briefly described in Appendix A.

Figure 3 visualizes the complex relationships between the physics involved in the proposed viscoelectromechanics model, and introduces the corresponding mathematical descriptors. In the material configuration, Ω_0, the external loading $\boldsymbol{P}$ is applied over the passive component (blue large external spring), the two sets of oriented active fibers (red internal contractile elements), and the viscous components (green internal dashpot). The active mapping $\boldsymbol{F}^a$, causing the contraction of the two active internal springs through an electric stimulation induced by the electric field $\boldsymbol{E}$, deforms the system into the active intermediate configuration Ω_a. In general, the modified length of the two contractile elements does not satisfy geometrical compatibility. The active part of the Helmholtz potential produces the active stress $\boldsymbol{P}^a$. The non compatible configuration stimulates the dashpot and the external spring, that work in a combined manner to reach the final compatible and balanced configuration. Viscous and elastic deformation gradients change in time, and at intermediate times it is possible to refer to a dissipative intermediate configuration Ω_v characterized by a rate of deformation $\boldsymbol{D}^v$. The dissipative configuration differs from Ω_a through the viscous deformation gradient $\boldsymbol{F}^v$ and from the spatial configuration through the elastic deformation gradient $\boldsymbol{F}^a$, and is characterized by the equilibrium stress $\boldsymbol{P}^E = \boldsymbol{P}^e + \boldsymbol{P}^v + \boldsymbol{P}^a$. The final configuration Ω is reached when the viscous rate of deformation, and the viscous stress $\boldsymbol{P}^v$, goes to zero. Thus, the equilibrium stress in the material configuration equals the sum of passive and active stress $\boldsymbol{P}^p + \boldsymbol{P}^a$; its counterpart in the spatial description corresponds to the Cauchy stress σ.

5. Case study: Human colon peristalsis

Now we specialize the coupled material model to reproduce intestine peristalsis, by adopting a specific and simplified form of the intestine electrophysiology. Then we apply the theory to describe the electromechanical behavior of a portion of the human colon, which geometry has been obtained through a semiautomatic segmentation of colonoscopy images. The numerical model of the intestine is characterized by the presence of two sets of fibers with local orientations $\boldsymbol{a}_1$ and $\boldsymbol{a}_2$, respectively. This choice is in line with the anatomical intestine description provided in Section 2.

5.1. *Intestine electrophysiology*

In our numerical application we use a simplified model of electrical activity for mammalian small intestine that accounts for the interaction of fast and slow waves [42]. The electrical activity is restricted to two cell systems, i.e.,

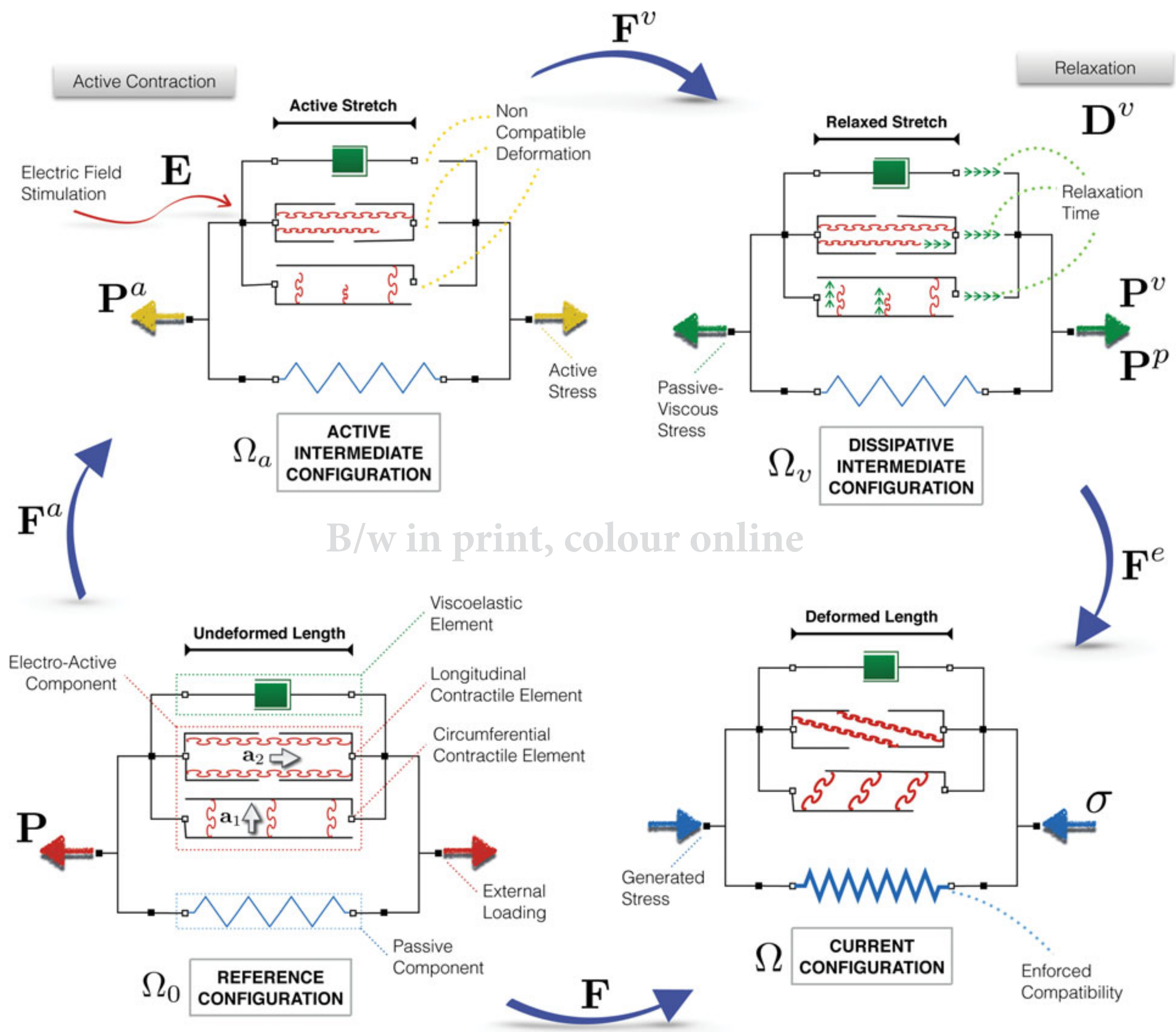

Figure 3. Schematic diagram of the different physics considered in the viscous electromechanical model and explaining the corresponding model symbology.

the LM and the ICC. According to this approach, the general nonlinear electric dynamics in Eq. (3) is described in each cell system by a pair of partial reaction-diffusion equations [43]. Equations involve two variables per system, u_j and v_j, defining dimensionless transmembrane potentials and slow currents, respectively, in the current configuration Ω. Membrane voltage is mapped back to physical dimensions as

$$u_l = \frac{V_l - V_{l,m}}{V_{l,M} - V_{l,m}}, \qquad u_i = \frac{V_i - V_{i,m}}{V_{i,M} - V_{i,m}},$$

where V_l is the dimensional transmembrane potential of the LM layer, $V_{l,m}$ and $V_{l,M}$ are the minimum and maximum physiological values of the same potential, respectively; V_i, $V_{i,m}$, and $V_{i,M}$ are the corresponding variables for the ICC layer. In the spatial version of Eq. (3), the four reaction-diffusion equations are given by

$$\frac{\partial u_l}{\partial t} = \boldsymbol{h}_{E,l} + I_{E,u_l}, \qquad \frac{\partial v_l}{\partial t} = I_{E,v_l}, \tag{13}$$

$$\frac{\partial u_i}{\partial t} = \boldsymbol{h}_{E,i} + I_{E,u_i}, \qquad \frac{\partial v_i}{\partial t} = I_{E,v_i} \tag{14}$$

where indices l, i refer to the LM and ICC variables, respectively. The spatial fluxes $\boldsymbol{h}_{E,j}$ and currents I_{E,u_j}, I_{E,v_j} specialize as

$$\begin{aligned}
\boldsymbol{h}_{E,l} &= -D_l \nabla u_l, \quad \boldsymbol{h}_{E,i} = -D_i \nabla u_i, \\
I_{E,u_l} &= -v_l + f(u_l) + F_l(u_l, u_i), \\
I_{E,v_l} &= \varepsilon_l [\gamma_l (u_l - \beta_l) - v_l], \\
I_{E,u_i} &= -v_i + g(u_i) + F_i(u_l, u_i), \\
I_{E,v_i} &= \varepsilon_i(z) [\gamma_i (u_i - \beta_i) - v_i].
\end{aligned}$$

where ∇^2 denotes the Laplace operator. The recovery variables show dependence in time, and the coupling between

Table 1. Parameters of the nondimensional intestine electrophysiological model [27, 42].

$k_l = 10$	$a_l = 0.06$	$\beta_l = 0$	$\gamma_l = 8$	$\varepsilon_l = 0.15$	$\alpha_l = 1$	$D_{li} = 0.3$	$D_l = 0.4$
$k_i = 7$	$a_i = 0.5$	$\beta_i = 0.5$	$\gamma_i = 8$	$\varepsilon_i = \varepsilon_i\,(z)$	$\alpha_i = -1$	$D_{il} = 0.3$	$D_i = 0.04$
[s^{-1}]	[-]	[-]	[s^{-1}]	[-]	[cm^{-2}]	[s^{-1}cm^2]	[s^{-1}cm^2]

the variables is expressed through the four functions

$$\begin{aligned} f\,(u_l) &= k_l u_l\,(u_l - a_l)\,(1 - u_l)\,, \\ F_l\,(u_l, u_i) &= \alpha_l D_{li}\,(u_l - u_i) \\ g\,(u_i) &= k_i u_i\,(u_i - a_i)\,(1 - u_i)\,, \\ F_i\,(u_l, u_i) &= \alpha_i D_{il}\,(u_l - u_i)\,. \end{aligned}$$

The two nonlinear functions $f\,(u_l)$ and $g\,(u_i)$ represent the cubic Zel'dovich's terms that arise in many contests for excitable tissues [26]. In particular, the β parameter shifts the bistable equilibrium point of the system from the null-cline position; $F_l\,(u_l, u_i)$ and $F_i\,(u_l, u_i)$ complete the coupling of the systems connecting the four equations in similar but opposite manner. Quantities D_l, D_i, D_{li}, D_{il} are the constant inter- intralayer diffusivity coefficients and, in this applications, are fine tuned to mimic a strong coupling within the LM layer but a weaker coupling between the two layers within the ICC layer, see Table 1. To complete the model, the ICC layer is characterized by an excitability parameter $\varepsilon_i(z)$ function of the distance from pylorus, i.e., the z-axis:

$$\varepsilon_i\,(z) = 0.032 + 0.05\exp\,(-z)\,. \tag{15}$$

The intestine wall is made by two fiber-reinforced material. By referring to the two principal anisotropy directions $\boldsymbol{a}_1$ and $\boldsymbol{a}_2$, the active part of the deformation gradient $\boldsymbol{F}^a$ is taken to assume the expression

$$\begin{aligned} \boldsymbol{F}^a = &\left(1 + \gamma_{\text{vol}}|\boldsymbol{E}|^2\right)\boldsymbol{I} + \gamma^1_{\text{dev}}(\boldsymbol{E}\cdot\boldsymbol{a}_1)^2\boldsymbol{a}_1\otimes\boldsymbol{a}_1 \\ &+\gamma^2_{\text{dev}}(\boldsymbol{E}\cdot\boldsymbol{a}_2)^2\boldsymbol{a}_2\otimes\boldsymbol{a}_2, \end{aligned} \tag{16}$$

where γ_{vol} and γ_{dev} are coefficient that describe the volumetric and the deviatoric active action, respectively. According to [9], we assume that the volumetric active strain derives from a normalized potential u_l defined as

$$\begin{aligned} u_{l_{\text{norm}}} &= \frac{u_l + 0.358}{1 + 0.358}, \\ f_{ul} &= 50\cdot\frac{1}{2}\text{atan}\left[300\log\left(\frac{0.1 - u_{l_{\text{norm}}}}{0.5}\right)\right], \\ \gamma_{\text{vol}} &= 0.37\frac{1.116}{1 + 0.0025\,f_{ul}} + 0.045. \end{aligned} \tag{17}$$

The functional parameters in (17) have been fine tuned to describe the intestine peristalsis activity [27]; see Table 2. This voltage describes an active strain that persists for a certain lapse of time after the electric potential wave crossing, in order to model the duration of the muscle contraction.

5.2. *Anisotropic viscoelasticity*

In the present application, we consider an expression of the viscoelastic Helmholtz strain energy density that accounts for anisotropy [6]:

$$A = A^e(\boldsymbol{F}^e, \boldsymbol{a}_1, \boldsymbol{a}_2) + A^v(\boldsymbol{F}^v) + A^a(\boldsymbol{F}, \boldsymbol{E}, \boldsymbol{a}_1, \boldsymbol{a}_2). \tag{18}$$

In particular, the elastic part A^e of the strain energy density has the form

$$\begin{aligned} A^e = &\frac{1}{2}KJ^{e2} + \mu_1\left(\overline{I}^e_1 - 3\right) + \mu_2\left(\overline{I}^e_2 - 3\right) \\ &+\sum_{n=1,2}\frac{k_n}{k_{n2}}\exp k_{n2}\left[\left(\overline{I}^e_{4n} - 1\right)^2 - 1\right], \end{aligned} \tag{19}$$

where $K,\ \mu_1,\ \mu_2,\ k_1,\ k_{12},\ k_2,\ k_{22}$ are material parameters, J^e is the determinant of $\boldsymbol{F}^e$, $\overline{I}^e_1,\ \overline{I}^e_2,\ \overline{I}^e_{41},\ \overline{I}^e_{42}$ are the first, second, and fourth invariants of the modified elastic Cauchy-Green deformation tensor $\overline{\boldsymbol{C}}^e = J^{e-2/3}\boldsymbol{C}^e$. Time-dependency is accounted for by defining a Newtonian viscosity dual dissipation potential of Neo-Hookean type [35]

$$\psi^* = J\left[\frac{1}{2}\,\zeta\ \text{tr}(\boldsymbol{D}^v)^2 +\ \eta\ \boldsymbol{D}^v\cdot\boldsymbol{D}^v\right],$$

with $J = \det\boldsymbol{F}$ and ζ and η volumetric and deviatoric viscosity parameters, respectively. Finally, the expression of the active part of the strain energy density is taken of the form [6]

$$A^a = -\frac{1}{2}J\epsilon_0\boldsymbol{E}\boldsymbol{F}^{-1}\cdot\left[\boldsymbol{I} + \boldsymbol{\chi}(\boldsymbol{C}, \boldsymbol{a}_1, \boldsymbol{a}_2)\right]\boldsymbol{F}^{-T}\boldsymbol{E}, \tag{20}$$

with

$$\begin{aligned} \boldsymbol{\chi}(\boldsymbol{C}, \boldsymbol{a}_1, \boldsymbol{a}_2) = &\left(\chi_{\text{iso}} + \chi^C_{\text{iso}}(I_1 - 3)\right)\boldsymbol{I} \\ &+\sum_{n=1,2}\left(\chi_{\text{fiber}} + \chi^C_{\text{fiber}}(I_{4n} - 1)\right)\boldsymbol{a}_n\otimes\boldsymbol{a}_n, \end{aligned} \tag{21}$$

Table 2. Anisotropic material model parameters used in the examples of applications of the viscous active electromechanical model fine tuned upon porcine experimental data [44].

K	μ_1	μ_2	k_4	k_{42}	k_6	k_{62}	ζ	η
[kPa]	[kPa]	[kPa]	[kPa]	[-]	[kPa]	[-]	[kPa s]	[kPa s]
5.5	1	1	55	56	20	29	0.125	0.09

χ_{iso}	χ_{fiber}	χ^C_{iso}	χ^C_{fiber}	γ^1_{dev}	γ^2_{dev}
[-]	[-]	[-]	[-]	[-]	[-]
1	5	3	12	−0.05	−0.05

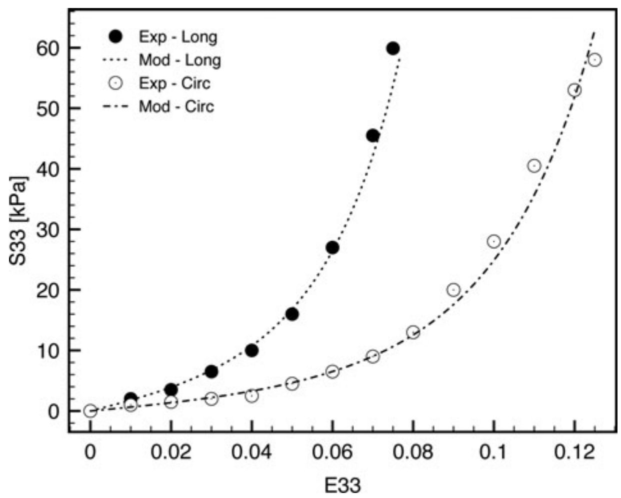

Figure 4. Equi-biaxial loading test. Comparison between uniaxial experimental data [44] (Exp) and passive constitutive material model (Mod) formulation (see Table 2). Test are performed in the direction of the longitudinal (Long) and circumferential (Circ) fibers. S33 and E33 are the normal components in the direction of the fibers of the Second Piola-Kirchooff stress and Green-Lagrange strain tensors, respectively.

where χ_{iso}, χ_{fiber}, χ^{C}_{iso}, χ^{C}_{fiber} are material parameters and I_1, I_{41}, I_{42} the first and fourth (in directions $\boldsymbol{a}_1$ and $\boldsymbol{a}_2$, respectively) invariants the total Cauchy-Green deformation tensor $\boldsymbol{C}$.

Passive material parameters were fine tuned upon porcine intestine biaxial testing documented in [44]. The calibration against the experimental results has been performed on the passive material model considering separately uniaxial loading in two different fiber directions. Thus, the coefficients μ_1, k_4, k_{42} have been calibrated for the longitudinal direction and the coefficients μ_2, k_6, k_{62} for the circumferential one, keeping the bulk modulus K constant. Uniaxial stress strain curves obtained during the identification of the parameters are shown in Figure 4. The values of the calibrated parameters, listed in Table 2, are in the range of magnitude of soft biomaterial parameters.

5.3. Customized colon geometry modeling

We refer to a three-dimensional solid model of human colon geometry reconstructed from 3D virtual colonoscopy images. We consider a 26 mm long anatomical section, with an average diameter of 23 mm, extracted from the central region of descending colon conduct. In order to reduce the complexity of the computational model, we did not model the internal soft layers and disregard the surrounding soft tissues that offer a compliant confinement to the intestine.

The computational mesh consists of 9,891 nodes and 38,646 tetrahedral finite elements; see Figure 5(a). At each integration point of the geometrical model we describe longitudinal and circumferential smooth muscle fibers, see Figure 5(b)–(c). The two ending cross-section of the computational mesh are constrained not to move in the direction of the longitudinal axis. The external and internal surfaces are traction free.

The active strain wave is computed according to the physiological model previously described, as originated by the sequence of two electric potential waves. The total duration of the process is 12 s, corresponding to two slow activation waves. We conducted two dynamic analyses, the first considering an inviscid behavior, the second one by accounting for viscosity of the material.

5.4. Numerical analysis

Figure 6 shows the propagation of the electric signal on the model assumed to be rigid. Autooscillatory propagating phenomena can be observed in the longitudinal direction. Due to the nonsymmetric geometry of the model,

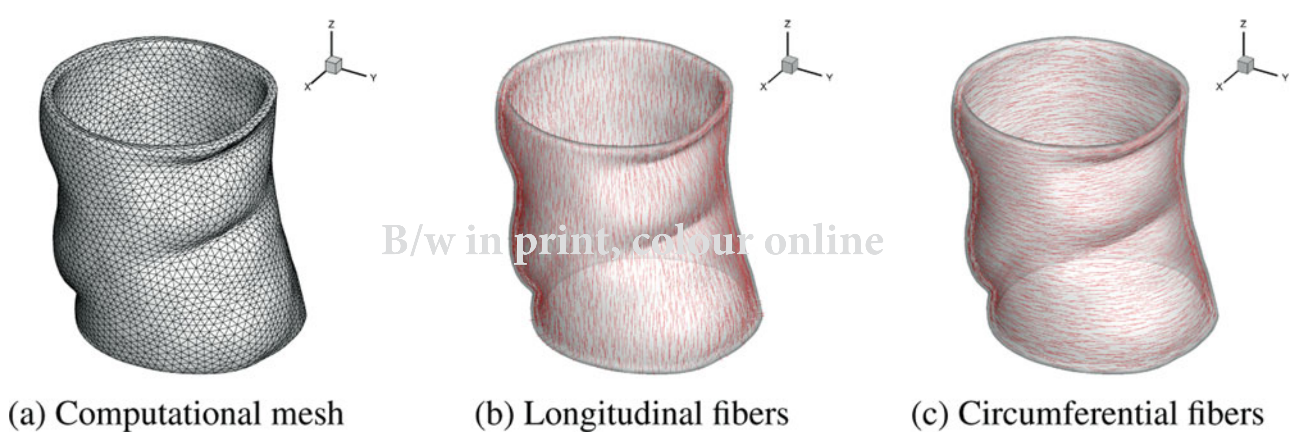

Figure 5. (a) Geometrical model and finite element discretization; (b) distribution of the longitudinal SMC (drawn 1/6 of total fibers); (c) distribution of the circumferential SMC (drawn 1/6 of total fibers).

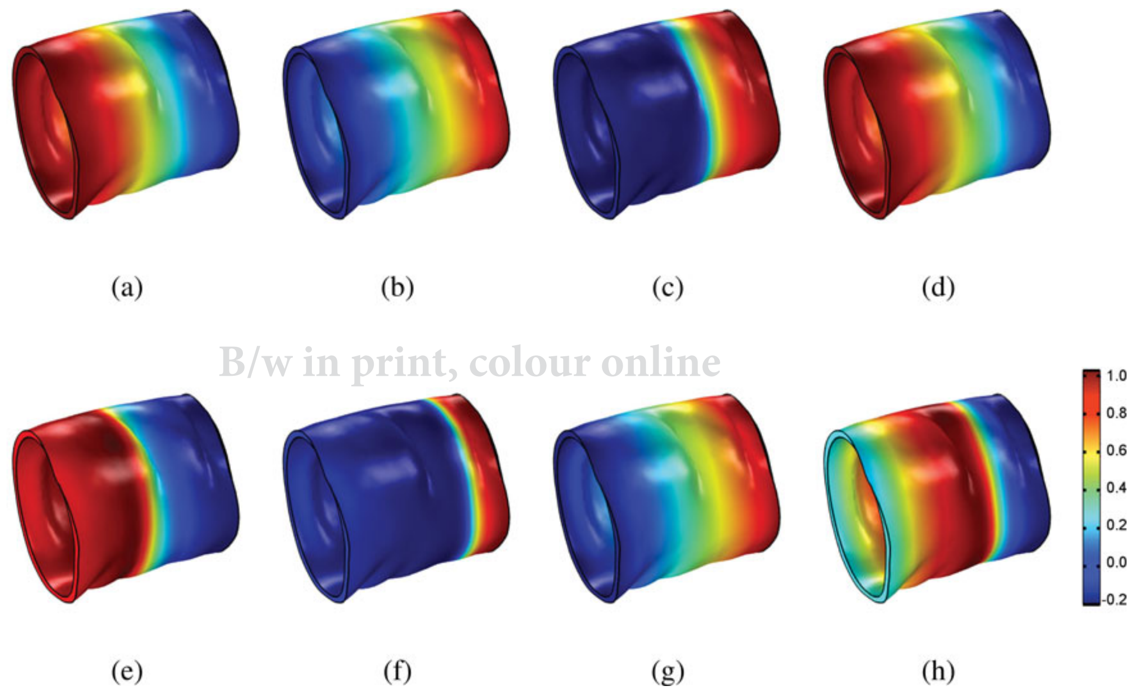

Figure 6. Purely electric peristaltic wave propagation. Consecutive frames with $\Delta t = 4$s. The color map refers to the nondimensional voltage membrane u_l. The peristaltic wave propagates from left to right.

the electric wave propagation is not characterized by concentric circular, regularly spaced, signals but by distorted and interrupted waves, as occurs in real conditions [45]. The effect of the electric activity is the contraction of the model in the circumferential direction along sections moving form one end to the other end of the model, reproducing the peristaltic motion of the intestine.

Numerical simulations show how the crossing of the electric wave causes the circumferential contraction of the segment of intestine, leading to a strong reduction of the intestine lumen. The contraction is followed by the expansion of the lumen, that regains the original size, after the completion of the wave cycle. In the case of the viscous behavior, the contraction and the expansion phase are delayed in time, thus the peristaltic motion is slowed down, and the stress level is also reduced. A comparison between the results of the numerical analyses for the purely elastic and the viscoelastic material models is shown in Figure 7. The images show the longitudinal stress distribution at the same time. In the case of

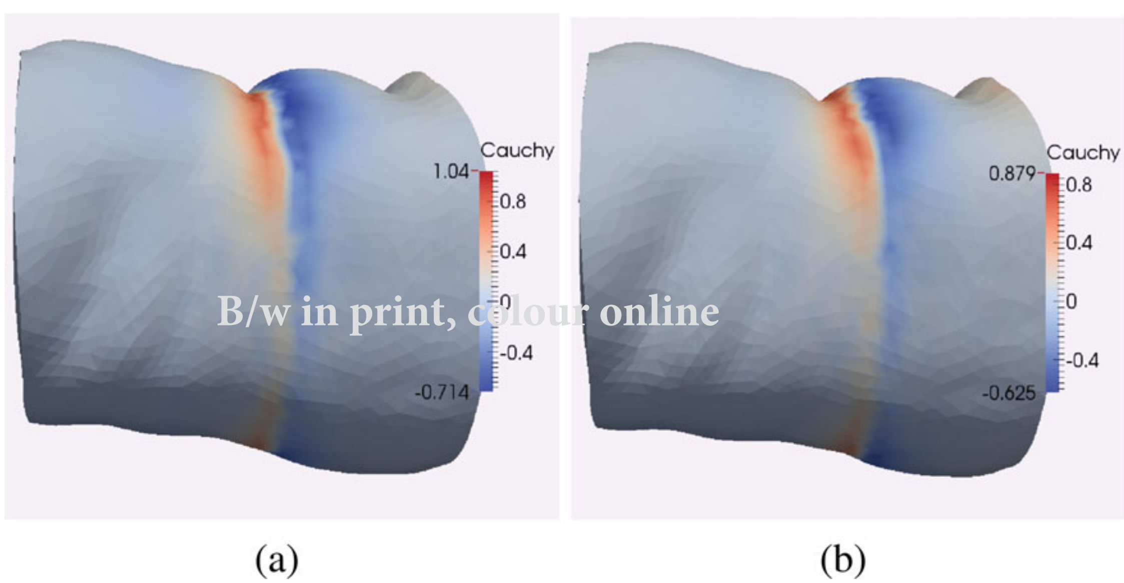

Figure 7. Numerical calculations. Stress distribution [MPa] at time of the maximum contraction. (a) Electroactive response. (b) Viscoelectroactive response.

the active elastic material, the longitudinal stress varies in the range [−0.714, 1.04] MPa; while in the case of the active viscoelastic material, it varies in the range [−0.625, 0.879] MPa.

6. Conclusions

This work presented a general theoretical framework for viscous electroactive soft materials considering the classical additive decomposition of the Helmholtz free energy density in elastic, viscous, and active parts. We accompanied the additive splitting of the energy with a multiplicative decomposition of the deformation gradient tensor in elastic, viscous, and active part, in view of formulating a specific multiphysics coupling for soft viscous active media. The viscous behavior has been included through an ideal standard solid equivalent considering Newtonian viscosity. The general model, formulated in finite kinematics, has been specialized in view of a numerical application, consisting in the simulation of the electromechanical behavior of intestine walls.

In particular, in this work we analyzed the peristalsis of a limited portion of the human intestine, using material parameters fine tuned upon experimental biaxial data acquired from the recent literature [44]. In our simulations, the passive behavior accounts for the presence of smooth muscle fibers oriented both in longitudinal and circumferential directions. The resulting model is a realistic three-dimensional structure characterized by a nontrivial anisotropic response. The electrophysiology characterizing the active part has been adapted from the excitation-contraction coupling usually adopted in cardiac electromechanics [9].

Using a customized three-dimensional geometry model of human colon, processed by means of a semiautomatic segmentation of MRI images and subsequent refinement of the numerical domain, we conducted three different quasistatic evolutive analyses: (i) purely electric, (ii) electromechanical, and (iii) viscoelectromechanical. Simulations showed that viscosity is of relevance in the description of the intestine peristalsis, since the level of the stress is overall reduced and the contraction induced by the electric signal is released after much longer times.

The specific constitutive coupling laws adopted in the general theoretical framework, together with a fine tuning of the active and passive material parameters, allowed us to reproduce with good accuracy the peristaltic motion of the intestine wall with and without viscous effects. In particular, we reproduced the electrical activation timing of the tissue based on slow wave evidences [23]. The induced deformation, then, reproduced the typical intestine wall deformation of more than 30% of its resting length [46].

In currently going-on work, we are improving the theoretical model by modeling the intestine electrophysiological function with a more realistic description of the typical complex nonlinear dynamics [47] and by considering microstructural arrangement of the tissue constituents [20]. Furthermore, we want to consider the nonlinear feedback due environmental coupling, e.g., and the presence of temperature gradients [27, 29]. Internal soft layers, i.e., mucosa, submucosa and villi, will be included in a future structural model of the intestine wall, with the aim of characterizing the full multiscale architecture of the system. Damage approaches [48] and collagen fiber recruitment [49] will be also taken into account in a multiphysics and multiscale generalization of the model. Validation of the extended model based on recent in vivo noninvasive measurement techniques [24] and on mechanical responses of single cells by using intracellular magnetic nanorods [50] will be the object of future studies. Finally, high performance computing schemes will be explored for efficient model applications and reliable modeling predictions [51].

Acknowledgments

AG and AP acknowledge the support from Gruppo Nazionale per la Fisica Matematica (GNFM). AG also acknowledges the support of the Istituto Nazionale di Alta Matematica (INdAM) under the Young Researcher 2014 grant. AG thanks the Gastroenterology Unit and the Department of Radiology, University Campus Bio-Medico of Rome for providing him with colonoscopy images and useful discussions.

References

1. L. D. Landau, E. M. Lifshitz, and L. P. Pitaevskii, *Electrodynamics of Continuous Media*, vol. 8, Butterworth-Heinemann, Oxford, 1984.
2. R. W. Ogden and D. Steigman, *Mechanics and Electrodynamics of Magneto- and Electro-elastic Materials*, CISM International Centre for Mechanical Sciences, Springer, Udine, 2011.
3. A. Ask, A. Menzel, and M. Ristinmaa, On the Modelling of Electro-Viscoelastic Response of Electrostrictive Polyurethane Elastomers, IOP Conf. Ser.: Mater. Sci. Eng., vol. 10, p. 012101, IOP Publishing Ltd, Bristol, UK, 2010.
4. A. Ask, A. Menzel, and M. Ristinmaa, Phenomenological Modeling of Viscous Electrostrictive Polymers, Int. J. Non-Linear Mech., vol. 47, pp. 156–165, 2012.
5. A. Ask, A. Menzel, and M. Ristinmaa, Electrostriction in Electro-Viscoelastic Polymers, Mech. Mater., vol. 50, pp. 9–21, 2012.
6. A. Gizzi, C. Cherubini, S. Filippi, and A. Pandolfi, Theoretical and Numerical Modeling of Nonlinear Electrome-Chanics With Applications to Biological Active Media, Commun. Comput. Phys., vol. 17, pp. 93–126, 2015.

7. F. Ravelli, Mechano-Electric Feedback and Atrial Fibrillation, Progr. Biophys. Mol. Biol., vol. 82, pp. 137–149, 2003.
8. N. Kuijpers, H. ten Eikelder, P. Bovendeerd, S. Verheule, T. Arts, and P. Hilbers, Mechanoelectric Feedback Leads to Conduction Slowing and Block in Acutely Dilated Atria: A Modeling Study of Cardiac Electromechanics, Amer. J. Phys. Heart Circulat. Physiol., vol. 292, pp. H2832–2853, 2007.
9. C. Cherubini, S. Filippi, P. Nardinocchi, and L. Teresi, An Electromechanical Model of Cardiac Tissue: Constitutive Issues and Electrophysiological Effects, Prog. Biophys. Mol. Biol., vol. 97, pp. 562–573, 2008.
10. W. Flügge, *Viscoelasticity*, Springer-Verlag, Heidelberg, Berlin, 1975.
11. Y. C. Fung, Foundations of Solid Mechanics, Prentice-Hall Inc., Englewood Cliffs, New Jersey, USA, 1965.
12. P. Ciarletta and M. Ben Amar, A Finite Dissipative Theory of Temporary Interfibrillar Bridges in the Extracellular Matrix of Ligaments and Tendons, J. R. Soc. Interface, vol. 6, pp. 909–924, 2009.
13. E. Fancello, J. P. Ponthot, and L. Stainier, A Variational Formulation of Constitutive Models and Updates in Non-Linear Finite Viscoelasticity, Int. J. Numer. Method. Eng., vol. 65, pp. 1831–1864, 2006.
14. K. Hasanpour, S. Ziaei-Rad, and M. Mahzoon, A Large Deformation Framework for Compressible Viscoelastic Materials: Constitutive Equations and Finite Element Implementation, Int. J. Plastic., vol. 25, pp. 1154–1176, 2009.
15. M. A. Hassan, M. Hamdi, and A. Noma, The Nonlinear Elastic and Viscoelastic Passive Properties of Left Ventricular Papillary Muscle of a Guinea Pig Heart, J. Mech. Behav. Biomed. Mater., vol. 5, pp. 99–109, 2012.
16. Y. Hu, Viscoelasticity and Poroelasticity in Elastomeric Gels, Acta Mech. Solida Sinica, vol. 25, pp. 441–458, 2012.
17. P. Saxena, M. Hossain, and P. Steinmann, A Theory of Finite Deformation Magneto-Viscoelasticity, Int. J. Solid. Struct., vol. 50, pp. 3886–3897, 2013.
18. A. Javili, A. McBride, and P. Steinmann, Thermomechanics of Solids With Lower-Dimensional Energetics: On the Importance of Surface, Interface, and Curve Structures at the Nanoscale. A Unifying Review, Appl. Mech. Rev., vol. 65, p. 010802, 2013.
19. T. Q. Suo and Z. G. Lu, Large Conversion of Energy in Dielectric Elastomers by Electromechanical Phase Transition, Acta Mech. Sinica, vol. 28, pp. 1106–1114, 2012.
20. M. Bol, A. Schmitz, G. Nowak, and T. Siebert, A Three-Dimensional Chemo-Mechanical Continuum Model for Smooth Muscle Contraction, J. Mech. Behav. Biomed. Mater., vol. 13, pp. 215–229, 2012.
21. S. C. Murtada, A. Arner, and G. A. Holzapfel, Experiments and Mechanochemical Modeling of Smooth Muscle Contraction: Significance of Filament Overlap, J. Theor. Biol., vol. 297, pp. 176–186, 2012.
22. B. Sharifimajd and J. Stalhand, A Continuum Model for Excitation-Contraction of Smooth Muscle Under Finite Deformations, J. Theor. Biol., vol. 355, pp. 1–9, 2014.
23. W. E. J. P. Lammers, L. Ver Donck, J. A. J. Schuurkes, and B. Stephen, Longitudinal and Circumferential Spike Patches in the Canine Small Intestine in vivo, Amer. J. Phys., vol. 285, pp. G1014–G1027, 2003.
24. S. Somarajan, N. D. Muszynski, L. K. Cheng, L. A. Bradshaw, T. C. Naslund, and W. O. Richards, Non-Invasive Biomagnetic Detection of Intestinal Slow Wave Dysrhythmias in Chronic Mesenteric Ischemia, American J. Physiol. Gastrointestine Liver Physiol., (doi: 10.1152/ajpgi.00466.2014).
25. D. Maughan, J. Moore, J. Vigoreaxu, B. Barnes, and L. A. Mulieri, Work Production and Work Absorption in Muscle Strip From Vertebrate Cardiac and Insect Flight Muscle Fibers, Adv. Exp. Med. Biol., vol. 453, pp. 471–480, 1998.
26. D. Bini, C. Cherubini, S. Filippi, A. Gizzi, and P. E. Ricci, On Spiral Waves Arising in Natural Systems, Commun. Comput. Phys., vol. 8, pp. 610–622, 2010.
27. A. Gizzi, C. Cherubini, S. Migliori, R. Alloni, R. Portuesi, and S. Filippi, On the Electrical Intestine Turbulence Induced by Temperature Changes, Phys. Byol., vol. 7, p. 016011, 2010.
28. W. J. Lammers, Arrhythmias in the Gut, Neurogastroenterol. Motility, vol. 25, pp. 353–357, 2013.
29. A. Altomare, A. Gizzi, M. P. L. Guarino, A. Loppini, A. Cocca, M. Dipaola, R. Alloni, S. Cicala, and S. Filippi, Experimental Evidences and Mathematical Modeling of Thermal Effects on Human Colonic Smooth Muscle Contractility, Amer. J. Physiol. Gastrointest. Liver Phys., vol. 307, pp. G77–G88, 2014.
30. Z. Suo, Theory of Dielectric Elastomers, Acta Mechanica Solida Sinica, vol. 23, no. 6, pp. 549–578, 2010.
31. B. D. Coleman and W. Noll, The Thermodynamics of Elastic Materials With Heat Conduction and Viscosity, Arch. Rational Mech. Anal., vol. 13, no. 1, pp. 167–178, 1963.
32. J. Lubliner, On the Thermodynamic Foundations of Non-linear Solid Mechanics, Int. J. Non-Linear Mech., vol. 7, pp. 237–254, 1972.
33. R. M. McMeeking, C. M. Landis, and M. A. Jimenez, A Principle of Virtual Work for Combined Electrostatic and Mechanical Loading of Materials, Int. J. Non-Linear Mech., vol. 42, pp. 831–838, 2007.
34. K. Hutter, A. van de Ven, and A. A. F. Ursescu, Electromagnetic Field Matter Interactions in Thermoelastic Solids and Viscous Fluids, Springer-Heidelberg, 2006.
35. Q. Yang, L. Stainier, M. Ortiz, A Variational Formulation of the Coupled Thermo-Mechanical Boundary-Value Problem for General Dissipative Solids, J. Mech. Phys. Solids, vol. 54, pp. 401–424, 2006.
36. E. K. Rodriguez, A. Hoger, and A. D. McCulloch, Stress-Dependent Finite Growth in Soft Elastic Tissues, J. Biomech., vol. 27, pp. 455–467, 1994.
37. V. A. Lubarda, Constitutive Theories Based on the Multiplicative Decomposition of Deformation Gradient: Thermoelasticity, Elastoplasticity, and Biomechanics, Appl. Mech. Rev., vol. 57, no. 2, pp. 95–108, 2004.
38. D. Ambrosi, G. Arioli, F. Nobile, and A. Quarteroni, Electromechanical Coupling in Cardiac Dynamics: The Active Strain Approach, SIAM J. Appl. Math., vol. 71, no. 2, pp. 605–621, 2011.
39. M. Ortiz and L. Stainier, The Variational Formulation of Viscoplastic Constitutive Updates, Comput. Method. Appl. Mech. Eng., vol. 171, pp. 419–444, 1999.
40. P. Underwood, Dynamic Relaxation, in T. Belytschko, T. J. R. Hughes (eds.), *Computational Methods for Transient Dynamic Analysis*, Elsevier Science Publishers, Amsterdam, 1983, pp. 245–265.

41. D. R. Oakley and N. F. J. Knight, Adaptive Dynamic Relaxation Algorithm for Non-Linear Hyperelastic Structures, Comput. Method. Appl. Mech. Eng., vol. 126, pp. 67–89, 1995.
42. R. R. Aliev, A. W. Richards, and J. P. Wikswo, A Simple Nonlinear Model of Electrical Activity in the Intestine, J. Theor. Biol., vol. 204, pp. 21–28, 2000.
43. D. E. Hurtado and D. Henao, Gradient Flows and Variational Principles for Cardiac Electrophysiology: Toward Efficient and Robust Numerical Simulations of the Electrical Activity of the Heart, Comput. Method. Appl. Mech. Eng., vol. 273, pp. 238–254, 2014.
44. C. Bellini, P. Glass, M. Sitti, and E. S. Di Martino, Biaxial Mechanical Modeling of the Small Intestine, J. Mech. Behavior Biomed. Mater., vol. 4, pp. 1727–1740, 2011.
45. W. E. J. P. Lammers, B. Stephen, and S. M. Karam, Functional Reentry and Circus Movement Arrhythmias in the Small Intestine of Normal and Diabetic Rats, Amer. J. Physiol. Gastrointest. Liver Phys., vol. 302, pp. G684–G689, 2012.
46. L. K. Cheng, G. O'Grady, P. Du, J. U. Egbuji, J. A. Windsor, and A. J. Pullan, Gastrointestinal System, Wiley Interdisciplinary Rev.: Systems Biol. Med., vol. 2, pp. 65–79, 2010.
47. Y. C. Poh, A. Corrias, N. Cheng, and M. L. Buist, A Quantitative Model of Human Jejunal Smooth Muscle Cell Electrophysiology, Plos ONE, vol. 7, p. e42385, 2012.
48. B. Calvo, M. M. A. Pen a, E., and M. Doblare, An Uncoupled Directional Damage Model for Fibred Biological Soft Tissues. Formulation and Computational Aspects, Int. J. Numer. Method. Eng., vol. 69, pp. 2036–2057, 2007.
49. A. Gizzi, M. Vasta, and A. Pandolfi, Modeling Collagen Recruitment in Hyperelastic Bio-Material Models With Statistical Distribution of the Fiber Orientation, Int. J. Eng. Sci., vol. 78, pp. 48–60, 2014.
50. M. Castillo, R. Ebensperger, D. Wirtz, M. Walczak, D. E. Hurtado, and A. Celedon, Local Mechanical Response of Cells to the Controlled Rotation of Magnetic Nanorods, J. Biomed. Mater. Res.: Part B – Appl. Biomater., vol. 102, pp. 1779–1785, 2014.
51. R. Ruiz-Baier, A. Gizzi, S. Rossi, C. Cherubini, A. Laadhari, S. Filippi, and A. Quarteroni, Mathematical Modelling of Active Contraction in Isolated Cardiomyocytes, Math. Med. Biol., vol. 31, pp. 259–283, 2014.

Appendix A

We refer to the constitutive updates in the incremental form [35, 39] where the deformation process is considered at discrete times t_n, and denotes the free energy density at time t_n

$$A_n = A(\boldsymbol{F}^e_n, \boldsymbol{F}_n, \boldsymbol{E}_n, \boldsymbol{F}^\upsilon_n).$$

An incremental variational update at the time t_{n+1} can be formulated by introducing the incremental work of deformation function f_n which includes the dual dissipation potential contribution

$$f_n(\boldsymbol{F}^e{}_{n+1}, \boldsymbol{F}_{n+1}, \boldsymbol{E}_{n+1}, \boldsymbol{F}^\upsilon_{n+1}) = A_{n+1} + \Delta t\, \psi^*(\boldsymbol{D}_{n+1}, \boldsymbol{E}_{n+1}) - A_n, \qquad \text{(A.1)}$$

where

$$\boldsymbol{D}_{n+1} = \frac{1}{2} \frac{\log\left(\boldsymbol{F}_n^{\upsilon-T} \boldsymbol{C}^\upsilon_{n+1} \boldsymbol{F}_n^{\upsilon-1}\right)}{\Delta t}$$

is the discrete form of the incremental logarithmic viscous strain, and $\boldsymbol{C}^\upsilon = \boldsymbol{F}^{\upsilon\,T} \boldsymbol{F}^\upsilon$ is the viscous right Cauchy-Green deformation tensor. By replacing (10) in (A.1), we obtain:

$$\begin{aligned} &f_n(\boldsymbol{F}^e_{n+1}, \boldsymbol{F}_{n+1}, \boldsymbol{E}_{n+1}, \boldsymbol{F}^\upsilon{}_{n+1}) \\ &\quad = A^e(\boldsymbol{F}^e_{n+1}) + A^\upsilon(\boldsymbol{F}^\upsilon_{n+1}, \boldsymbol{E}_{n+1}) + A^a(\boldsymbol{F}_{n+1}, \boldsymbol{E}_{n+1}) \\ &\qquad + \Delta t\, \psi^*(\boldsymbol{D}_{n+1}, \boldsymbol{E}_{n+1}) - A_n. \end{aligned}$$

The updated viscous deformation $\boldsymbol{F}^\upsilon{}_{n+1}$ follows from the minimum principle [35, 39]:

$$\begin{aligned} &W_n(\boldsymbol{F}^e_{n+1}, \boldsymbol{F}_{n+1}, \boldsymbol{E}_{n+1}) \\ &\quad = \min_{\boldsymbol{F}^\upsilon{}_{n+1}} f_n(\boldsymbol{F}^e_{n+1}, \boldsymbol{F}_{n+1}, \boldsymbol{E}_{n+1}, \boldsymbol{F}^\upsilon{}_{n+1}). \end{aligned} \qquad \text{(A.2)}$$

It follows that the Euler-Lagrange equations for the problem (A.2) define the configurational equilibrium equations:

$$\begin{aligned} &\frac{\partial f_n(\boldsymbol{F}^e_{n+1}, \boldsymbol{F}_{n+1}, \boldsymbol{E}_{n+1}, \boldsymbol{F}^\upsilon{}_{n+1})}{\partial \boldsymbol{F}^\upsilon{}_{n+1}} \\ &\quad = -\boldsymbol{Y}^e_{n+1} - \boldsymbol{Y}^\upsilon_{n+1} - \boldsymbol{Y}^a_{n+1} - \boldsymbol{Y}^d_{n+1} = \boldsymbol{0}, \\ &\quad \times \boldsymbol{Y}^d_{n+1} = -\Delta t \frac{\partial \psi^*_n}{\partial \boldsymbol{F}^\upsilon{}_{n+1}}. \end{aligned} \qquad \text{(A.3)}$$

Eq. (A.3) can be solved, e.g., by a Newton-Raphson iteration. The requisite linearization of (A.3) is:

$$\frac{\partial f_n}{\partial \boldsymbol{F}^\upsilon{}_{n+1}} + \frac{\partial^2 f_n}{\partial \boldsymbol{F}^\upsilon{}_{n+1}\, \partial \boldsymbol{F}^\upsilon{}_{n+1}} \Delta \boldsymbol{F}^\upsilon{}_{n+1} \approx \boldsymbol{0}. \qquad \text{(A.4)}$$

Thus, the relation to be used at iteration $K+1$ is

$$\boldsymbol{F}^\upsilon{}_{K+1} = \boldsymbol{F}^\upsilon{}_K - \left[\left(\frac{\partial^2 f_n}{\partial \boldsymbol{F}^\upsilon{}_{n+1}\, \partial \boldsymbol{F}^\upsilon{}_{n+1}}\right)^{-1}\right]_K \left(\frac{\partial f_n}{\partial \boldsymbol{F}^\upsilon}\right)_K.$$

The explicit expression of the Hessian of f_n will not be in general available, therefore the inversion of the Hessian must be done numerically once the components have been computed.